A 9,9'-spirobifluorene bases Metal-Organic Framework: systhesis, structure analysis and gas sorption properties

Florian Moreau, Nathalie Audebrand, Cyril Poriel, Virginie Moizan-Baslé, Jean Ouvry

Journal of Materials Chemistry

Cite this: J. Mater. Chem., 2011, 21, 18715

www.rsc.org/materials

PAPER

A 9,9′-spirobifluorene based Metal–Organic Framework: synthesis, structure analysis and gas sorption properties†

Florian Moreau,[a] Nathalie Audebrand,*[a] Cyril Poriel,*[a] Virginie Moizan-Baslé[b] and Jean Ouvry[b]

Received 21st June 2011, Accepted 19th September 2011
DOI: 10.1039/c1jm12859k

The new square planar tetracarboxylate ligand L (4,4′,4″,4‴-(9,9′-spirobi[fluorene]-2,2′,7,7′-tetrayl) tetrabenzoic acid) was synthesized and used for synthesis of the Metal–Organic Framework $Cu_2L(H_2O)_2\cdot(EtOH)_4$ denoted SBF–Cu. This material possesses the classical 4–4 regular tiling topology with paddle-wheel inorganic building units. Due to the presence of SBF cores, the interactions between the layers of this MOF confer it specific properties: high specific surface area, open metal sites under activation, and promising hydrogen uptake capacity.

Introduction

Among the field of porous materials, Metal–Organic Frameworks (MOFs) have attracted great attention due to their potential applications[1–3] in gas storage,[4,5] molecule separation,[6,7] catalysis,[8–10] or drug delivery.[11] A proper choice of ligands and metals and the application of the concepts of building units[12] and scale chemistry[13] allow a chemical control of topology, pore size, and adsorption properties of the synthesized MOFs. The broad panel of commercially available ligands already gave rise to a large variety of MOFs. Nevertheless, as the combination of MOF porosity and crystallinity with other tunable features[14] is strongly sought worldwide for various applications, it remains highly important to develop original ligands with specific properties to be incorporated in such systems.

In this context, we designed a novel ligand based on the spirobifluorene (SBF) core. Indeed, although first synthesized in the 1930s,[15] SBF derivatives have experienced a fantastic development in the last twenty years. This rapid development of the SBF platform is mainly due to its application in organic electronics, leading to fantastic breakthrough in the field,[16] and also for its use as chiral ligand,[17,18] as electropolymerizable building block,[19,20] as solid state laser[21] or in third-order nonlinear optics.[22]

SBF can be considered as the joining of two fluorene units through a shared spiro carbon.[16] The two fluorene units are hence maintained in orthogonal planes in a resulting *D2d* symmetry (Fig. 1). Thus, attaching various molecular fragments to the rigid perpendicular fluorene units of SBF allows generating controlled connecting directions, a key commitment for designing open frameworks. Moreover, SBF derivatives are known to be highly thermally and morphologically stable and more soluble than their non-spiro analogues.[16] Despite all these appealing characteristics and the recent applications of the SBF core in microporous polymeric systems[23–25] and in molecular tectonics,[26–28] the incorporation of SBF in a MOF is almost absent from the literature. Indeed, to the best of our knowledge, only three coordination polymers using the SBF core as linking motif have been reported to date.[29–31] However, none of them shows permanent porosity.

The present study deals with the first porous coordination polymer based on the SBF backbone, extended with four aryl groups bearing the widely used carboxylate functions. The choice of the carboxylate function is justified by its well-known versatility to generate many bridging and chelating coordination modes.[32] This copper containing MOF, called SBF–Cu, shows classical 4–4 regular tiling topology with interesting properties compared to topologically similar MOFs:[33] high specific surface area, generation of open metal sites, and significant H_2 adsorption capacity. Herein, we hence report the design and the synthesis of a novel SBF-based ligand and its use in the synthesis of the MOF SBF–Cu. Crystal structure, topology analysis,

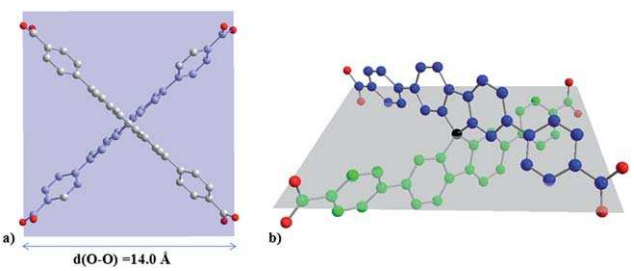

Fig. 1 (a) The square planar geometry of L. (b) Representation of its two curved arms (in blue and green) linked by the spiro carbon (in black) and mean plane of the ligand (in grey) in the crystal structure of SBF–Cu.

[a]*Sciences Chimiques de Rennes UMR 6226 CNRS, Université de Rennes 1, France. E-mail: nathalie.audebrand@univ-rennes1.fr; cyril.poriel@univ-rennes1.fr*
[b]*IFP Energies Nouvelles, Solaize, France*

† Electronic supplementary information (ESI) available: NMR, IR, UV-Vis spectra, EDS analysis, XRPD, selected bonds and angles, and useful figures. CCDC 831047. For ESI and crystallographic data in CIF or other electronic format see DOI: 10.1039/c1jm12859k

structure analogies with related MOFs and thermal behaviour are disclosed as well as N_2 and H_2 sorption properties.

Experimental

General techniques, materials and methods

Commercially available reagents and solvents were used without further purification other than those detailed below. Light petroleum refers to the fraction with bp 40–60 °C. Dichloromethane was distilled from P_2O_5 drying agent Sicapent (Merck). Semiconductor grade toluene has been used. Reactions were stirred magnetically. Analytical thin layer chromatography was carried out using aluminium backed plates coated with Merck Kieselgel 60 GF254 and visualized under UV light (at 254 and/or 365 nm). Chromatography was carried out using silica 60A CC 40–63 mm (SDS). ^{1}H and ^{13}C NMR spectra were recorded using Bruker 300 MHz instruments (^{1}H frequency, corresponding ^{13}C frequency is 75 MHz); chemical shifts were recorded in ppm and *J* values in Hz. The residual signals for the NMR solvents are: $CDCl_3$; 7.26 ppm for the proton and 77.00 ppm for the carbon, [D_6]DMSO; 2.50 ppm for the proton and 39.52 ppm for the carbon. The following abbreviations have been used for the NMR assignment: s for singlet, d for doublet, t for triplet, m for multiplet and br for broad.

Infrared spectra of all synthesized compounds have been recorded using a Varian 640-IR FT-IR spectrometer in the range 400–4000 cm^{-1}. High-resolution mass spectra were recorded at the Centre Regional de Mesures Physiques de l'Ouest (Rennes) on a Bruker MicrO-Tof-Q2 and reported as *m*/*z*. Names of chemicals have been determined according to systematic nomenclature rules agreed upon by the International Union of Pure and Applied Chemistry.

Synthesis

9,9′-Spirobi[fluorene] (**1**) was synthesized according to published procedures.[34] The spectroscopic analyses and purity of **1** were in perfect accordance with the literature.[35]

2,2′,7′7′-Tetrabromo-9,9′-spirobi[fluorene] (2). Neat bromine (30.3 mmol, 1.56 mL) was added to compound **1** (3.79 mmol, 1.20 g) dissolved in dichloromethane (160 mL) in a Schlenk tube. The resulting mixture was degassed and stirred under an argon atmosphere at ambient temperature for 8 days. Neat bromine (7.57 mmol, 3.9 mL) was added twice after 3 and 6 days. Progression of the reaction was followed by ^{1}H NMR spectroscopy. The resulting mixture was washed with an aqueous solution of sodium bisulfite (80 g L^{-1}, 2 × 150 mL). The organic layer was separated, dried on magnesium sulfate, and the solvent removed *in vacuo* to afford compound **2** as a colorless solid (2.32 g, 97% yield). The spectroscopic analyses and purity of **2** were in perfect accordance with the literature.[36,37]

Tetramethyl 4,4′,4″,4‴-(9,9′-spirobi[fluorene]-2,2′,7,7′-tetrayl) tetrabenzoate (3). 2 (0.95 mmol, 600 mg), 4-(methoxycarbonyl) phenylboronic acid (4.75 mmol, 855 mg) and potassium carbonate (3.25 mmol, 450 mg) were added to a mixture of toluene and deionized water (70 mL/15 mL). The resulting mixture was degassed, stirred under an argon atmosphere and heated at 80 °C. While stirring at 80 °C, under argon stream, tri-*tert*-butylphosphine (0.26 mmol, 63 μL) (P(*t*-Bu)$_3$) and tris (dibenzylideneacetone)dipalladium (0.2 mmol, 180 mg) ($Pd_2(dba)_3$, CH_2Cl_2) were carefully added. The Schlenk tube was sealed and the resulting mixture was stirred at 80 °C under an argon atmosphere for 20 h. After the mixture was cooled to room temperature, a saturated aqueous solution of ammonium chloride (50 mL) was added and the resulting mixture was extracted with dichloromethane (3 × 80 mL). The combined extracts were dried on magnesium sulfate, and the solvent removed *in vacuo*. Purification by column chromatography on silica gel eluting with light petroleum/ethyl acetate (7 : 3) gave compound **3** as a colorless solid (480 mg, 56% yield).

Mp > 300 °C; ^{1}H NMR: (300 MHz, $CDCl_3$) δ = 7.94 (d, *J* = 8.0 Hz, 4H, ArH), 7.92–7.86 (m, 8H, ArH), 7.65 (dd, *J* = 8.0, 1.7 Hz, 4H, ArH), 7.50–7.38 (m, 8H, ArH), 6.98 (d, *J* = 1.3 Hz, 4H, ArH), 3.81 ppm (s, 12H, Me); ^{13}C NMR: (75 MHz, $CDCl_3$) δ = 166.8 (C), 149.6 (C), 145.0 (C), 141.3 (C), 140.1 (C), 129.9 (CH), 128.8 (C), 127.6 (CH), 126.9 (CH), 122.8 (CH), 120.9 (CH), 66.2 (Cspiro), 52.1 ppm (Me); IR (*ν*): 1720 (C=O), 1606, 1466, 1433, 1403,1279 (C–O), 1248, 1188, 1105 (C–O), 1016, 860, 819, 770, 760, 704 cm^{-1}; UV-Vis (THF): λ_{max} = 323, 343 nm; HRMS (ESI$^+$, MeOH/CH_2Cl_2 90 : 10): *m*/*z* calcd for $C_{57}H_{40}O_8Na$: 875.2615 [M + Na$^+$]; found 875.2615.

4,4′,4″,4‴-(9,9′-Spirobi[fluorene]-2,2′,7,7′-tetrayl)tetrabenzoic acid (L). Sodium hydroxide (40 mmol, 1.6 g) was added to a suspension of **3** (0.56 mmol, 480 mg) in ethanol and deionized water (100 mL/15 mL). The resulting mixture was stirred under reflux for 12 h. After it was cooled to room temperature, ethanol was removed under vacuum. The resulting suspension was diluted with deionized water, acidified to pH = 2 using concentrated hydrochloric acid, and extracted with ethyl acetate (3 × 80 mL). The combined organic layers were dried on magnesium sulfate, the solvent was removed under vacuum to afford L as a colorless solid (440 mg, 99% yield).

Mp > 300 °C; ^{1}H NMR (300 MHz, DMSO-d_6): δ = 12.80 (sbr, 4H, COOH); 8.27 (d, *J* = 7.8 Hz, 4H, ArH); 7.87 (m, 12H, ArH); 7.59 (d, *J* = 7.8 Hz, 8H, ArH); 7.02 ppm (s, 4H, ArH); ^{13}C NMR: (75 MHz, DMSO-d_6) δ = 167.0 (C), 149.3 (C), 143.5 (C), 141.1 (C), 139.0 (C), 129.8 (CH), 129.5 (C), 127.4 (CH), 126.6 (CH), 121.8 (CH), 121.4 (CH), 65.8 ppm (Cspiro). IR (*ν*): 2976 (O–H), 2899 (O–H), 1686 (C=O), 1608, 1407, 1278 (C–O), 1248, 1178, 1018, 858, 829, 771, 750, 715 cm^{-1}; UV-Vis (THF): λ_{max} = 323, 342 nm; HRMS (ESI$^-$, MeOH/CH_2Cl_2 95 : 5): *m*/*z* calcd for $C_{53}H_{31}O_8$: 795.2024 [M − H$^-$]; found 795.2024.

SBF–Cu: $Cu_2L(H_2O)_2\cdot(EtOH)_4$. L (1.25 × 10^{-2} mmol, 10.0 mg) was dissolved in a solution of $CuCl_2\cdot 2H_2O$ in *N*,*N*′-dimethylformamide (2.5 mL, 0.01 M). Ethanol (2.5 mL) and hydrochloric acid aqueous solution (1 mL, 0.05 M) were added to the resulting solution, which was placed in a tightly capped PFA (perfluoroalkoxy copolymer resin) flask in an oven at 80 °C for 48 h. Small blue crystals were collected by filtration, washed with DMF and ethanol, and dried in air (65% yield based on formula deduced from TGA, see below); IR (*ν*): 2981, 2894, 1656, 1604, 1402, 1245, 1180, 1012, 862, 848, 823, 782, 760, 709 cm^{-1}. After activation of SBF–Cu (see gas sorption measurements) and rehydration upon exposure to standard conditions, Cu_2L

$(H_2O)_2 \cdot 4H_2O$ is obtained (SBFCu_act); IR (ν) 1606, 1402, 1247, 1218, 1186, 1014, 862, 846, 809, 781, 759, 732, 710 cm^{-1}. Elemental analysis: calcd: C, 61.93; H, 3.89; found: C, 59.84; H, 3.63%.

Energy dispersive spectroscopy (EDS)

EDS was performed on single-crystals of SBF–Cu at the Centre de Microscopie Électronique à Balayage et microAnalyse de l'Université de Rennes 1 on a JEOL JSM 6400 spectrometer, equipped with an Oxford Link Isis analyzer with a VARIAN SpectrAA 10 plus.

Single-crystal data collection

A suitable single-crystal of SBF–Cu was mounted on a four-circle APEX II Bruker-AXS diffractometer (Centre de Diffractométrie X, UMR CNRS 6226, Rennes), using Mo Kα radiation ($\lambda = 0.71073$ Å). Intensities were collected at 150 K by means of the program Bruker SMART included in the APEX2 programs suite.[38] Reflection indexing, Lorentz-polarization correction, peak integration and background determination were carried out with the program Bruker SAINT.[39] Unit-cell parameter refinement and frame scaling were performed with the program Bruker SMART.[38] Numerical absorption corrections were performed using a semi-empirical absorption correction included in the program SADABS.[40] The resulting sets of *hkl* reflections were used for structure refinement. Crystallographic data and details on data collection are listed in Table 1. Structure drawings were carried out with Diamond 3, supplied by Crystal Impact.[41]

Table 1 Crystallographic data and structure refinement parameters for SBF–Cu

Empirical formula	$CuC_{26.5}O_5H_{14}$
Molecular weight/g mol^{-1}	475.92
Crystal system	Monoclinic
Space group	*P*2/*c* (no. 13)
Z	4
a/Å	13.698(5)
b/Å	16.631(5)
c/Å	14.562(5)
V/Å^3	782.36(4)
β/°	95.825(5)
Calculated density/g cm^{-3}	0.958
Crystal size/mm^3	0.1 × 0.1 × 0.02
T/K	150
λ/Å	0.71073
θ range/°	1.22–27.62
Index ranges	$-17 \le h \le 14$, $-21 \le k \le 19$, $-18 \le l \le 18$
Unique data	7600
Observed data ($I > 2\sigma(I)$)	4842
Refinement method	Full-matrix least-squares on $\|F^2\|$
R_1 ($I > 2\sigma(I)$)	0.0490
R_1 (All)	0.0789
wR_2 ($I > 2\sigma(I)$)	0.1395
wR_2 (All)	0.1504
Goodness of fit	0.958
No. of variables	294
Largest difference map peak and hole/e Å^{-3}	0.455 and −0.524

X-Ray powder diffraction

X-Ray powder diffraction data of ground crystals of SBF–Cu were collected at room temperature with a Siemens D500 diffractometer, with the parafocusing Bragg-Brentano geometry, using monochromatic Cu Kα_1 radiation (λ =1.5406 Å) selected with an incident beam curved-crystal germanium monochromator.[42] The diffraction pattern was collected over the angular range 4–37° (2θ) with a counting time of 30 s per step and a step length of 0.015° (2θ). The extraction of the peak positions was carried out with the DIFFRAC Plus EVA software package supplied by Bruker AXS. Pattern indexing and refinement of the unit-cell parameters were performed with the program DICVOL06.[43] The powder diffraction data have been submitted to the ICDD[44] for inclusion in the Powder Diffraction File.

Temperature-dependent X-ray diffraction (TDXD) was performed in static air with a Bruker AXS D5005 powder diffractometer using a diffracted-beam graphite monochromator (Cu K$\alpha_{1,2}$), equipped with an Anton Paar HTK1200 oven camera. *In situ* measurements were carried out at various constant temperatures. Between each measurement step, the sample was heated at a rate of 1.0 °C min^{-1} to the desired temperature. Temperature calibration was made with standard materials in the involved temperature range. Diffraction patterns were collected over the angular range 4–25° (2θ) with a counting time of 5 s per step and a step length of 0.02° (2θ).

Structure determination of SBF–Cu

The crystal structure of the title compound was determined in the space group *P*2/*c* in agreement with the extinction conditions. The heavy atoms, as well as the whole ligand groups, were located by direct methods with the program SIR97.[45] The remaining H atoms of the ligand were localised from successive difference Fourier or calculated by the HFIX command with SHELXL-97[46] included in the WinGX platform.[47] The positions of the hydrogen atoms were refined with soft constraints applied to the distances to their C parent atoms [1.10(3) Å] and their isotropic displacement parameters were fixed equal to one and half times the U_{eq} value of the same C parent atoms. Details of the final refinement are given in Table 1. The selected bond distances and angles are reported in Table S1 (see ESI†).

The refinement of the framework was performed by ignoring the contribution of the disordered solvent molecules. The region containing the disordered electronic density was identified by considering the van der Waals radii of the atoms constitutive of the ordered framework. The contribution of this region to the total structure factor was calculated *via* a discrete Fourier transformation and subtracted in order to generate a new set of *khl* reflections by means of the program SQUEEZE included in the PLATON software.[48] This new set was used for further least-squares refinement.

Thermogravimetry

Thermogravimetric analysis (TGA) was performed on a Shimadzu TGA50 instrument in static air with a heating rate of 1.0 °C min^{-1} until 900 °C. The powdered samples (*ca.* 10 mg) of the as synthesized SBF–Cu ($Cu_2L(H_2O)_2 \cdot (EtOH)_4$) and activated

SBF–Cu_act ($Cu_2L(H_2O)_2 \cdot 4H_2O$) were spread in alumina crucibles.

Gas sorption measurements

Prior to any measurement, a 70 mg sample of SBF–Cu was degassed at 373 K under secondary vacuum (10^{-4} mbar) for 10 hours. In order to determine BET and Langmuir specific surface areas and micropore volume, N_2 adsorption at 77 K was studied on a Micromeritics ASAP2010 instrument. Hydrogen adsorption capacity at 77 K was determined using a Bel Japan Belsorp-max apparatus.

Results and discussion

Synthesis of L: 4,4′,4″,4‴-(9,9′-spirobi[fluorene]-2,2′,7,7′-tetrayl)tetrabenzoic acid

The synthesis of the target ligand is presented in Scheme 1. A catalyst free bromination of **1**, synthesized according to the literature procedure,[34] has been carried out, smoothly and cleanly leading to **2** with 97% yield. It should be noted that bromination of **1** can also be carried out using ferric chloride as catalyst with a stoichiometric amount of bromine (75% yield). However, this reaction appears to be difficult to control and highly sensitive to the amount of bromine and the dryness of ferric chloride. With the bromo analogue **2** in hand, the next step was to introduce the four aryl arms. This has been achieved through the Suzuki–Miyaura cross-coupling reaction with 4-(methoxycarbonyl)phenylboronic acid. However, the reactivity of the bromine atoms appears to be poor and only low yields of **3** were obtained when using common catalysts such as $Pd(PPh_3)_4$ or $PdCl_2$(dppf), CH_2Cl_2. After intensive scouting, the best catalytic conditions found were to use $Pd_2(dba)_3$ and CH_2Cl_2/P(*t*-Bu)$_3$ as catalytic system and potassium carbonate as the base in a mixture of toluene and water (3/1) leading to **3** with 56% yield. Finally, hydrolysis of the methyl carboxylate groups easily leads to the tetracarboxylic acid L with a quantitative yield. This new route is efficient (overall yield of 54%), simple, performed in smooth conditions, and appears to be highly adaptable to synthesize tetracarboxylate SBF-based ligands.

Preparation and preliminary characterisations of SBF–Cu

With the tetracarboxylic acid L in hand, a new organic/inorganic framework was synthesized in a mixture of DMF, EtOH and H_2O under mild conditions. It should be noted that the synthesis of MOFs very often involves the use of DMF as a solvent, and the present synthesis does not infringe the rule. Indeed, it has been suggested that the slow hydrolysis of DMF molecules into dimethylamine is a crucial parameter for the deprotonation of the carboxylic acid ligands and then for the control of the growth of the hybrid crystals.[49,50]

As a first assessment of the formation of a hybrid material, preliminary experiments were carried out. The C : Cu ratio deduced from EDS analysis on single-crystals of SBF–Cu (see Table S2 in the ESI†) is 23, indicating a ligand/metal ratio roughly equal to 2, in accordance with the crystal structure (see below) and with the elemental analysis results. Infrared spectroscopy of powdered sample of SBF–Cu shows the ν_{as} and ν_s vibration bands of the deprotonated carboxylate groups of the ligand, respectively, at 1605 and 1398 cm^{-1}, and no ν(C=O) vibration band from DMF molecules could be observed (see Fig. S7 in the ESI†).

Comparison between the X-ray powder diffraction pattern of the bulk product and a simulated pattern from the crystal structure further described shows reasonable agreement (Fig. 2). The few discrepancies might be explained by a different content of the pores and/or by preferred orientation. The diffraction lines were indexed with a monoclinic unit-cell, with the following refined parameters: $a = 13.458(4)$ Å, $b = 16.962(6)$ Å, $c = 14.595(6)$ Å, $\beta = 94.50(3)°$, and $V = 3321$ Å^3 [$M_{20} = 17$, $F_{30} = 56$ (0.0091, 39)]. These parameters are in agreement with those found from X-ray single-crystal diffraction (Table 1).

Description of the crystal structure of SBF–Cu

General geometry of the ligand L. The ligand 4,4′,4″,4‴-(9,9′-spirobi[fluorene]-2,2′,7,7′-tetrayl)tetrabenzoic acid L is constituted by the joining through a spiro carbon atom of two orthogonal aryl/fluorene/aryl "arms", bearing in the *para* position of each aryl group a carboxylic acid function, leading to upper and lower arms. The upper arm is curved down, and the lower arm is curved up, so that the four carboxylate functions are not strictly, but almost coplanar. In addition, the four carbon atoms of these carboxylate functions are all 0.52 Å distant from the mean plane of the molecule. Finally, the ligand can be considered as a square-planar Building Unit (BU) with a 14.0 Å long side (Fig. 1).

Crystal structure description of SBF–Cu. SBF–Cu crystallizes in the space group *P*2/*c* (Table 1). The asymmetric unit consists of one "half" of the ligand with its spiro carbon sitting on the two-fold axis (Wyckoff position 2e), a Cu^{2+} cation, and a water molecule (Fig. S14, see ESI†). The inorganic BUs of the framework are the so-called copper paddle-wheels $Cu_2(R\text{-}COO)_4(H_2O)_2$. The two Cu^{2+} cations are situated in a regular square pyramidal geometry generated by space-group symmetry, with four equatorial carboxylic functions from independent SBF ligands bridging the two ions (Cu–O bond length range: 1.950–1.962 Å) and two apical water molecules (Cu–O: 2.177 Å) (see

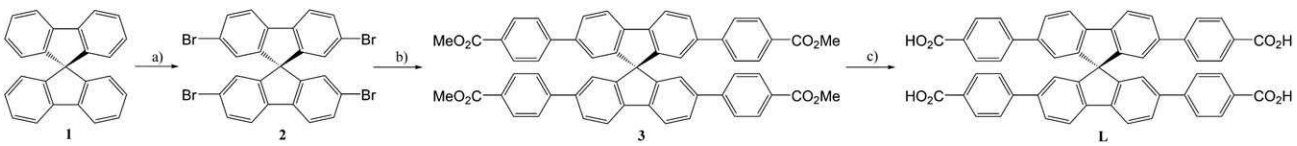

Scheme 1 Synthesis of L. (a) Br_2/CH_2Cl_2, 25 °C, 97%; (b) 4-(methoxycarbonyl)phenylboronic acid, [Pd_2dba_3], P(*t*-Bu)$_3$, K_2CO_3, THF/H_2O, 80 °C, 56%; and (c) NaOH, H_2O/EtOH, reflux, 99%.

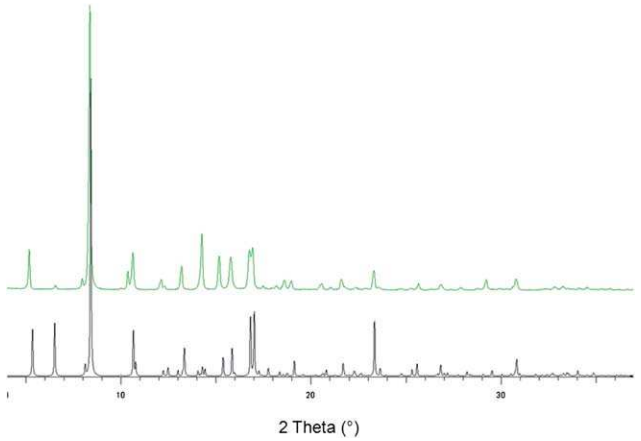

Fig. 2 X-Ray Powder diffraction pattern of SBF–Cu. Black: simulated from single crystal structure. Green: experimental pattern.

Table S1 in the ESI†). Since both organic and inorganic BUs have a square planar geometry, the resulting framework consists of a 2D square planar grid with a 4–4 regular tilling topology. The grids are piled up in an AA manner, generating 1D, 16.6 Å wide channels along the *c* axis, which contain the disordered solvent molecules. Due to the curve of each arm of the SBF ligand, the rows of the grid are corrugated, alternating up and down arms (Fig. 3).

An interesting feature of SBF–Cu concerns its topology and pore diameter. The 4–4 topology has been previously encountered for other paddle-wheel based MOFs with 1D pore diameters in the same range as those of SBF–Cu. Indeed, Zn(1,4-BDC)·(DMF)(H_2O) (1,4-BDC = 1,4-benzenedicarboxylate) also known as MOF-2[51] and its topoisomer Cu(1,4-BDC)·(DMF)[52,53] present structural features very similar to those of SBF–Cu. Actually, the SBF core plays the same square planar topological role as that of a paddle-wheel in the MOF-2 structure (Fig. 4). Both materials possess square planar building units connected through one-dimensional "rods": *para*-benzoate groups of L in SBF–Cu and terephthalate linkers in MOF-2. In addition, the distance C6–C19 (6.9 Å) in SBF–Cu (see Fig. S14 in the ESI†) is comparable to the distance between two opposite equatorial carbonyl carbon atoms of a paddle-wheel (5.2 Å) in MOF-2. Consequently, the two materials present very similar 1D pore diameters (MOF-2: *d*(Zn–Zn) = 15.4 Å, SBF–Cu: *d*(Cu–Cu) = 16.6 Å, see Fig. 4). Additionally, pilling of the layers must be compared. The average distances between the layers are 5.46 Å and 6.14 Å and the shortest distances between two copper atoms from neighbour layers are 4.83 Å and 5.32 Å for MOF-2 and SBF–Cu, respectively.

On one hand, within both crystal structures of SBF–Cu and MOF-2, the cohesion of the layers is due to hydrogen bonds between the apical water molecules and carboxylate oxygen atoms of the adjacent layer (Fig. 5a). On the other hand, in MOF-2, the large distance between aromatic rings of the adjacent layers (>6 Å) forbids the existence of π-stacking interactions. Oppositely, in SBF–Cu, the proximity of the conjugated aryl–fluorene–aryl arms of two adjacent layers allows potential interactions between the two π systems (Fig. 5b). In the low temperature crystal structure of SBF–Cu, two aromatic rings

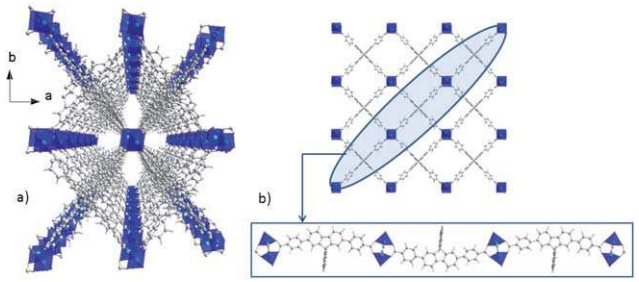

Fig. 3 Crystal structure of SBF–Cu: (a) central projection view showing channels along the [001] direction; (b) representation of a single grid and one of its corrugated rows. Solvent molecules have been omitted for clarity.

belonging to two distinct neighbor ligands (denoted B′ and C in Fig. S12, see ESI†) could be involved in π-stacking interactions.

As discussed by Janiak,[54] the strength of the hypothetical π-stacking interactions between two aromatic rings can be evaluated by measuring three parameters: the centroid–centroid distance (distance between two ring centroids), the ring slippage angles (the angle between the normal projection of one ring centroid on the other ring and the centroid–centroid vector), and the vertical displacement (distance between the centroid of one ring and the normal projection of the centroid of the other) (see Fig. S11 in the ESI†). For centroid–centroid distances longer than 4.0 Å along with large slippage angles (>30°) and vertical displacements (>2 Å), the π-stacking interactions are usually considered as medium to weak.[55]

In the case of SBF–Cu, the centroid–centroid distance is 4.12 Å, the vertical displacement is 2.85 Å, and the slippage angles are 34.6°. Such values indicate that weak π-stacking interactions can contribute to the cohesion between the layers, additionally to hydrogen bonds.

π–π interactions have been reported for the paddle-wheel based MCF-23 which also possesses 4–4 topology.[55] Interestingly, in MCF-23 as well as in SBF–Cu, proximity between π systems of adjacent layers is allowed by the use of a curved ligand generating corrugated grids.

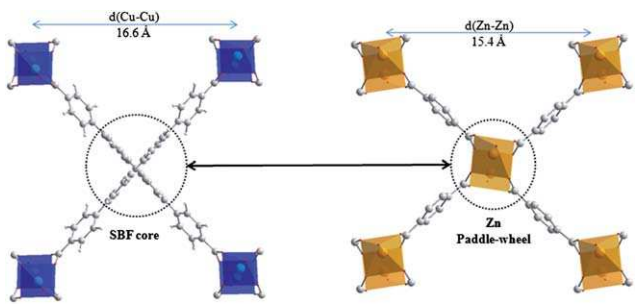

Fig. 4 Comparison of the topologies and pore sizes of (a) SBF–Cu and (b) MOF-2.

Thermal behavior and activation process of SBF–Cu

The structure of $Cu_2L(H_2O)_2\cdot(EtOH)_4$ comprises 47.6% of solvent accessible void, as calculated by the SQUEEZE

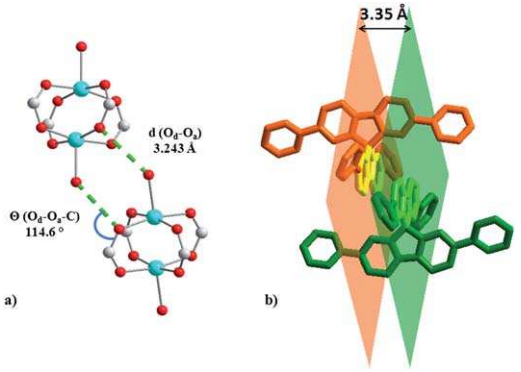

Fig. 5 Non covalent interactions in SBF–Cu: (a) hydrogen bonds between two adjacent paddle-wheels; (b) representation of adjacent ligand arms involved in π-stacking within the crystal structure of SBF–Cu.

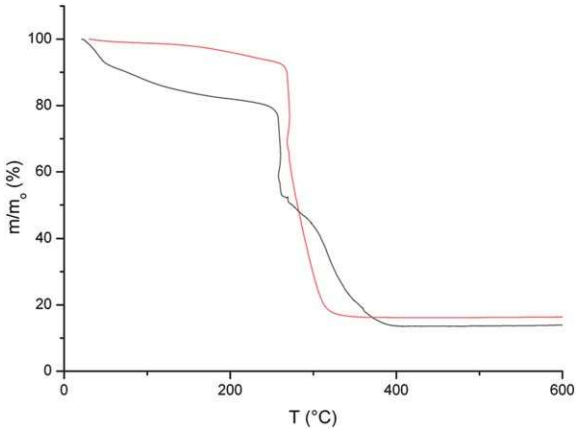

Fig. 6 TG curves of SBF–Cu (black line) and SBF–Cu_act (red line).

program. Hence, this compound exhibits a rather open framework. $Cu_2L(H_2O)_2\cdot(EtOH)_4$ is stable upon departure of the crystallization solvent molecules under heat treatment.

Indeed, TGA of the crude product SBF–Cu shows a weight loss of 19% starting at ambient temperature which is consistent with the presence of 4 ethanol crystallisation solvent molecules per formula unit, which affords $Cu_2L(H_2O)_2$. This 19% loss is absent from the thermogram of the MOF after preliminary heat treatment. It should be noted that a 6.5% mass loss remains, which is consistent with a re-uptake of 4 water molecules per formula unit after desolvation and exposition to air. The decomposition of the ligand (64%) starts around 250 °C, leading to the final crystalline product CuO (Fig. 6).

In order to study the thermal behavior of SBF–Cu during elimination of its solvent molecules, TDXD studies were carried out. SBF–Cu remains crystalline up to 200 °C (Fig. 7) before its decomposition into CuO, which is in agreement with the TG experiment. During the heating process, only slight shifts of the diffraction peaks can be observed. In particular, the (002) reflection shows the largest shift in 2θ from 12.16° at ambient temperature to 11.58° at 200 °C. The c axis is almost perpendicular to the 2D square planar grids. Then, an increase of the spacing between the grids can be supposed.

Surprisingly, MOF-2 and the isostructural MOF Cu(1,4-BDC)·(DMF) show a drastically different thermal behavior. Indeed these materials undergo a clear phase transition around 170 °C.[51,52] The authors have postulated that the high temperature phase consists of a condensed structure where apical solvent molecules of the paddle-wheels have been evacuated, leading to a connection of the grids through M–O–M links. This type of condensation of the layers does not take place in SBF–Cu and a slight opposite phenomenon even happens since the inter-grid distance is believed to increase. The reason for such a difference, despite the similarity of the topologies of these MOFs, is necessarily the preexisting π-stacking interactions between the layers in SBF–Cu inhibiting their condensation, even after removal of the apical water molecules of the paddle-wheels. This hypothesis is strengthened by the behavior of SBF–Cu_act during final activation, which is realized by heating the material to 100 °C under vacuum during 10 hours before gas sorption measurements. During this treatment, the color of the compound changes drastically, turning from bluish green to deep blue (Fig. 8). This is attributed to the departure of the coordinated apical water molecules. The corresponding change in the coordination sphere of the Cu cations generates Lewis acid copper sites also called open metal sites in the activated and dehydrated material SBF–Cu_oms. This color change is reversible, the material turns back to green when exposed to atmospheric pressure, ambient temperature or humidity, and the material SBF–Cu_act remains crystalline after gas sorption measurements (see Fig. S13 in the ESI†). This phenomenon has been extensively described and studied for the well known MOF HKUST-1.[56–58] Such open metal sites are quite rare among paddle-wheel based 2D MOFs with a 4–4 topology. Indeed, to the best of our knowledge only one comparable material has been reported so far: $[Cu_2(bdc)_2(DMF)]H_2O\cdot(DMF)(C_2H_5OH)_{0.5}$ (bdc = 1,3-benzenedicarboxylate).[59] In this case, van der Waals interactions are involved between the layers, whereas in the case of SBF–Cu, the ability to create unsaturated metal centers depends on the interactions between the π systems of the SBF ligands from neighbor layers.

N_2 and H_2 sorption properties

In order to assess the permanent porosity of the activated material, SBF–Cu_oms was subjected to N_2 adsorption analysis

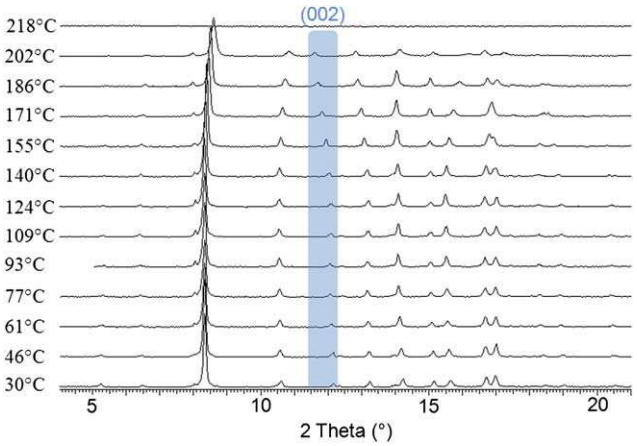

Fig. 7 TDXD patterns of SBF–Cu.

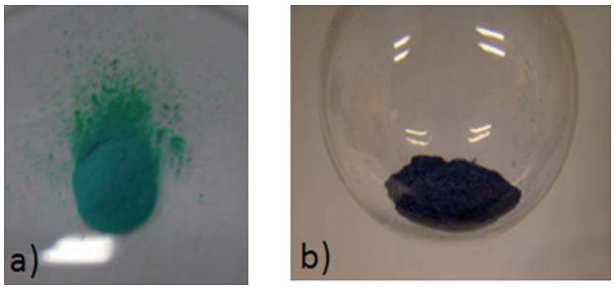

Fig. 8 Pictures of (a) SBF–Cu_act (activated) and (b) SBF–Cu_oms (with open metal sites) in a BET cell.

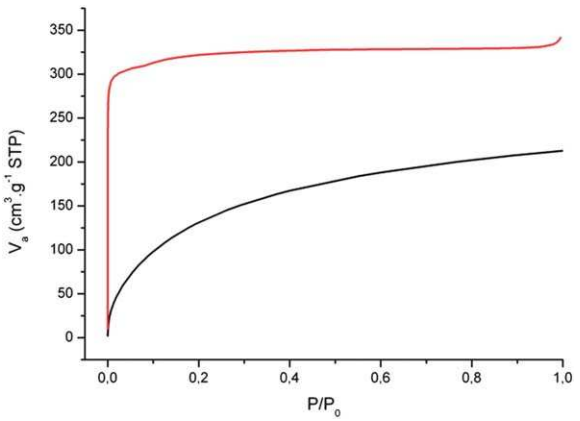

Fig. 9 N_2 (red line) and H_2 (black line) adsorption isotherms of SBF–Cu_oms.

at 77 K. The adsorption isotherm shows a typical type I behaviour (Fig. 9, red line), with BET and Langmuir specific surface areas of 1116 $m^2\ g^{-1}$ and 1427 $m^2\ g^{-1}$, respectively, and a micropore volume of 0.498 $cm^3\ g^{-1}$. These values are significantly higher than those reported for MOF-2,[51] Cu(1,4-BDC)·(DMF)[52,53] and $[Cu_2(bdc)_2(DMF)]H_2O\cdot(DMF)(C_2H_5OH)_{0.5}$.[59] This porosity enhancement can be partly explained by the lower density of SBF–Cu_act due to its lower metal content.

Since MOFs with open metal sites are promising candidates for hydrogen storage,[60] the hydrogen adsorption in SBF–Cu_oms was finally investigated. Thus an H_2 uptake of 1.77 wt% was measured at 77 K and 1 atm (Fig. 9, black line). In order to evaluate the influence of open-metal on H_2 storage capacity of SBF–Cu_oms, it should be compared to other topologically similar MOFs, but to the best of our knowledge, such studies have not been reported so far.

Conclusions

In summary, we have reported the synthesis, crystal structure, thermal behaviour and gas sorption properties of the first porous MOF based on a new SBF tetracarboxylate ligand. The crystal structure of SBF–Cu is built from corrugated layers with a 4–4 tiling topology whose nodes are occupied alternatively by copper paddle-wheels and SBF cores.

The most striking feature of the present framework is the pilling of the layers leading to π–π interactions and creation of open metal sites under activation of the material. Moreover, among the MOFs with the paddle-wheel based 4–4 framework, SBF–Cu possesses the highest S_{BET} reported to date and its H_2 adsorption capacity at 77 K and 1 atm is in the value range expected for a material with such porosity.

Acknowledgements

Grateful thanks are expressed to Dr T. Roisnel (Centre de Diffractométrie, UMR CNRS 6226) for his assistance in single-crystal data collection, Damien Thirion (Sciences Chimiques de Rennes UMR 6226 CNRS, Université de Rennes1) for his fruitful advices in organic chemistry, and to MENSR for financial support.

Notes and references

1 (*a*) *Metal–Organic Frameworks Design and Application*, ed. Leonard R. Mac-Gillivray, John Wiley & Sons, Hoboken, 2010; (*b*) *Chem. Soc. Rev.*, Special Issue, 2009, **38**; (*c*) *Eur. J. Inorg. Chem.*, Special Issue, 2010, **24**.
2 (*a*) G. Férey, *Chem. Soc. Rev.*, 2008, **37**, 191; (*b*) S. Kitagawa, R. Kitaura and S. Naro, *Angew. Chem., Int. Ed.*, 2004, **43**, 2334.
3 U. Mueller, M. Schubert, F. Teich, H. Puetter, K. Schierle-Arndt and J. Pastré, *J. Mater. Chem.*, 2006, **16**, 626.
4 (*a*) X. Lin, J. Jia, X. Zhao, K. M. Thomas, A. J. Blake, G. S. Walker, N. R. Champness, P. Hubberstey and M. Schröder, *Angew. Chem., Int. Ed.*, 2006, **45**, 7358; (*b*) J. L. C. Rowsell and O. M. Yaghi, *Angew. Chem., Int. Ed.*, 2005, **44**, 4670; (*c*) J. Li, Y. Ma, M. C. McCarthy, J. Sculley, J. Yu, H. Jeong, P. B. Balbuena and H. Zhou, *Coord. Chem. Rev.*, 2011, **255**, 1791.
5 G. Férey, C. Serre, T. Devic, G. Maurin, H. Jobic, P. L. Llewellyn, G. De Weireld, A. Vimont, M. Daturi and J. Chang, *Chem. Soc. Rev.*, 2011, **40**, 550.
6 F. Millange, N. Guillou, M. E. Medina, G. Férey, A. Carlin-Sinclair, K. M. Golden and R. I. Walton, *Chem. Mater.*, 2010, **22**, 4237.
7 C. Serre, C. Mellot-Draznieks, S. Surblé, N. Audebrand, Y. Filinchuk and G. Férey, *Science*, 2007, **315**, 1828.
8 K. C. Szeto, C. Prestipino, C. Lamberti, A. Zecchina, S. Bordiga, M. Bjorgen, M. Tilset and K. P. Lillerud, *Chem. Mater.*, 2007, **19**, 211.
9 O. K. Farha, A. M. Shultz, A. A. Sarjeant, S. T. Nguyen and J. T. Hupp, *J. Am. Chem. Soc.*, 2011, **133**, 5652.
10 D. Farrusseng, S. Aguado and C. Pinel, *Angew. Chem., Int. Ed.*, 2009, **48**, 7502.
11 (*a*) P. Horcajada, C. Serre, M. Vallet-Regi, M. Sebban, F. Taulelle and G. Férey, *Angew. Chem., Int. Ed.*, 2006, **45**, 5974; (*b*) Z. Ma and B. Moulton, *Coord. Chem. Rev.*, 2011, **255**, 1623.
12 (*a*) M. O'Keeffe, M. Eddaoudi, H. Li, T. M. Reineke and O. M. Yaghi, *J. Solid State Chem.*, 2000, **152**, 3; (*b*) D. J. Tranchemontagne, J. L. Mendoza-Cortes, M. O'Keeffe and O. M. Yaghi, *Chem. Soc. Rev.*, 2009, **38**, 1257.
13 G. Férey, *J. Solid State Chem.*, 2000, **152**, 37.
14 D. Zhao, D. J. Timmons, D. Yuan and H.-C. Zhou, *Acc. Chem. Res.*, 2011, **44**, 123.
15 R. G. Clarkson and M. J. Gomberg, *J. Am. Chem. Soc.*, 1930, **52**, 2881.
16 T. P. I. Saragi, T. Spehr, A. Siebert, T. Fuhrmann-Lieker and J. Salbeck, *Chem. Rev.*, 2007, **107**, 1011.
17 J.-H. Xie and Q.-L. Zhou, *Acc. Chem. Res.*, 2008, **41**, 581.
18 C. Poriel, Y. Ferrand, P. Le Maux, J. Rault-Berthelot and G. Simonneaux, *Synth. Met.*, 2008, **158**, 796.
19 C. Poriel, Y. Ferrand, P. Le Maux, J. Rault-Berthelot and G. Simonneaux, *Chem. Commun.*, 2003, 1104.
20 C. Poriel, Y. Ferrand, P. Le Maux, J. Rault-Berthelot and G. Simonneaux, *Inorg. Chem.*, 2004, **43**, 5086.
21 D. Schneider, T. Rabe, T. Riedl, T. Dobbertin, M. Kröger, E. Becker, H.-H. Johannes, W. Kowalsky, T. Weimann, J. Wang, P. Hinze, A. Gerhard, P. Stössel and H. Vestweber, *Adv. Mater.*, 2005, **17**, 31.
22 S. Y. Kim, M. Lee and B. H. Boo, *J. Chem. Phys.*, 1998, **109**, 2593.
23 J. Weber and A. Thomas, *J. Am. Chem. Soc.*, 2008, **130**, 6334.
24 J. Weber, M. Antonietti and A. Thomas, *Macromolecules*, 2008, **41**, 2880.

25 J. Weber, Q. Su, M. Antonietti and A. Thomas, *Macromol. Rapid Commun.*, 2007, **28**, 1871.
26 J.-H. Fournier, T. Maris and J. D. Wuest, *J. Org. Chem.*, 2004, **69**, 1762.
27 E. Demers, T. Maris, J. Cabana, J.-H. Fournier and J. D. Wuest, *Cryst. Growth Des.*, 2005, **5**, 1237.
28 E. Demers, T. Maris and J. D. Wuest, *Cryst. Growth Des.*, 2005, **5**, 1227.
29 C. S. Collins, D. Sung, W. Liu, J.-L. Zuo and H.-C. Zhou, *J. Mol. Struct.*, 2008, **890**, 163.
30 P. K. Clews, R. E. Douthwaite, B. M. Kariuki, T. Moore and M. Taboada, *Cryst. Growth Des.*, 2006, **6**, 1991.
31 K.-T. Wong, Y.-L. Liao, Y.-C. Peng, C.-C. Wang, S.-Y. Lin, C.-H. Yang, S.-M. Tseng, G.-H. Lee and S.-M. Peng, *Cryst. Growth Des.*, 2005, **5**, 667.
32 C. N. R. Rao, S. Natarajan and R. Vaidhyanathan, *Angew. Chem., Int. Ed.*, 2004, **43**, 1466.
33 M. Köberl, M. Cokoja, W. A. Herrmann and F. E. Kühn, *Dalton Trans.*, 2011, **40**, 6834.
34 V. Prelog and D. Bedeković, *Helv. Chim. Acta*, 1979, **62**, 2285.
35 C. Poriel, Y. Ferrand, S. Juillard, P. Le Maux and G. Simonneaux, *Tetrahedron*, 2004, **60**, 145.
36 R. Wu, J. S. Schumm, D. L. Pearson and J. M. Tour, *J. Org. Chem.*, 1996, **61**, 6906.
37 J. Pei, J. Ni, X.-H. Zhou, X.-Y. Cao and Y.-H. Lai, *J. Org. Chem.*, 2002, **67**, 4924.
38 Bruker-Nonius, *SMART in APEX2 programs suite version 2.1-0*, Bruker AXS Inc., Madison, Wisconsin, USA, 2006.
39 Bruker-Nonius, *SAINT version 7.23A*, Bruker AXS Inc., Madison, Wisconsin, USA, 2005.
40 G. M. Sheldrick, *SADABS version 2.03*, Bruker AXS Inc., Madison, Wisconsin, USA, 2002.
41 K. Brandenburg and M. Berndt, *Diamond (version 3)*, Crystal Impact, Bonn, 2001.
42 D. Louër and J. I. Langford, *J. Appl. Crystallogr.*, 1988, **21**, 430.
43 D. Louër and A. Boultif, *Z. Kristallogr., Suppl.*, 2007, **2007**, 191.
44 International Centre for Diffraction Data, Newtown Square, PA.
45 A. Altomare, M. C. Burla, M. Camalli, G. Cascarano, C. Giacovazzo, A. Guagliardi, A. G. G. Moliterni, G. Polidori and R. Spagna, *J. Appl. Crystallogr.*, 1999, **32**, 115.
46 G. M. Sheldrick, *Acta Crystallogr., Sect. A: Found. Crystallogr.*, 2007, **64**, 112.
47 L. J. Farrugia, *J. Appl. Crystallogr.*, 1999, **32**, 837.
48 A. L. Spek, *PLATON, A Multipurpose Crystallographic Tool*, Utrecht university, Utrecht, The Netherlands, 2002.
49 L. Xie, S. Liu, B. Gao, C. Zhang, C. Sun, D. Li and Z. Su, *Chem. Commun.*, 2005, 2402.
50 A. D. Burrows, K. Cassar, R. M. W. Friend, M. F. Mahon, S. P. Rigbyb and J. E. Warrenc, *CrystEngComm*, 2005, **7**, 548.
51 H. Li, M. Eddaoudi, T. L. Groy and O. M. Yaghi, *J. Am. Chem. Soc.*, 1998, **120**, 8571.
52 C. G. Carson, K. Hardcastle, J. Schwartz, X. Liu, C. Hoffmann, R. A. Gerhardt and R. Tannenbaum, *Eur. J. Inorg. Chem.*, 2009, (16), 2338.
53 K. Seki, S. Takamizawa and W. Mori, *Chem. Lett.*, 2001, 122.
54 C. Janiak, *J. Chem. Soc., Dalton Trans.*, 2000, (21), 3885.
55 X. Wang, Y. Zhang, H. Huang, J. Zhang and X. Chen, *Cryst. Growth Des.*, 2008, **8**, 4559.
56 S. S. Y. Chui, S. M. F. Lo, J. P. H. Charmant, A. G. Orpen and I. D. Williams, *Science*, 1999, **283**, 1148.
57 K. Schlichte, T. Kratzke and S. Kaskel, *Microporous Mesoporous Mater.*, 2004, **73**, 81.
58 C. Prestipino, L. Regli, J. G. Vitillo, F. Bonino, A. Damin, C. Lamberti, A. Zecchina, P. L. Solari, K. O. Kongshaug and S. Bordiga, *Chem. Mater.*, 2006, **18**, 1337.
59 D. Xue, Y. Lin, X. Cheng and X. Chen, *Cryst. Growth Des.*, 2007, **7**, 1332.
60 M. Dinca and J. R. Long, *Angew. Chem., Int. Ed.*, 2008, **47**, 6766.

